Technical University of Denmark

DTU

A New Frequency Domain Autofocus

Dall, Jørgen

Published in:
International Geoscience and Remote Sensing Symposium

Publication date:
1991

Document Version
Publisher's PDF, also known as Version of record

Link back to DTU Orbit

DTU Library
Technical Information Center of Denmark

A NEW FREQUENCY DOMAIN AUTOFOCUS ALGORITHM FOR SAR

Jørgen Dall

Electromagnetics Institute
Technical University of Denmark
B 348, DK-2800 Lyngby, Denmark
Telephone: 45-42 88 14 44
Fax: 45-45 93 16 34
Telex: 37529 dthdia

ABSTRACT

A new autofocus algorithm with a very high computational efficiency is presented. Although based on a completely different principle, this "shift-and-correlate" algorithm has some similarity with the traditional map drift algorithm. Theory and preliminary tests indicate that the two algorithms have comparable accuracies. However, with the new algorithm the number of arithmetic operations is reduced by a factor of about 50. This, in combination with its non-iterative nature, makes it very suitable for real-time processing.

KEYWORDS: SAR, autofocus, real-time implementation.

INTRODUCTION

High resolution Synthetic Aperture Radar (SAR) imaging requires a detailed knowledge of the platform motion. In case of airborne SARs this knowledge is often based on an Inertial Navigation Unit (INU) preferably mounted next to the SAR antenna. However, the INU has a limited accuracy, and in particular drift is a problem. Therefore, even in cases where the SAR comprises an INU, it may be necessary to derive motion information directly from the SAR data.

The along track velocity drift is found by means of autofocus. A constant velocity error leads to a quadratic phase error, and hence to bad focusing. In the following, the quadratic phase error will be referred to as the along track velocity error, although a constant cross track acceleration also contributes.

With a Doppler bandwidth of B_D, an azimuth resolution of $\rho_a = v/B_D$ is attainable, but the velocity v should be known within

$$\rho_v = \pm \frac{v\rho_a^2}{\lambda R} \tag{1}$$

corresponding to a quadratic phase error of $\pi/4$. λ is the wavelength, and R is the range.

In the remainder of this paper the Doppler centroid is assumed to be zero, and only quadratic phase errors are considered (INU-based motion compensation). However, the autofocus algorithm presented is easily modified to take into account a non-zero Doppler centroid, and possibly it can be generalized to deal with higher order phase errors.

The autofocus algorithm to be presented is called "shift-and-correlate". Although based on a completely different principle, it has some similarity with the traditional map drift algorithm, which is described briefly, before the theory of the shift-and-correlate algorithm is developed. Next, a very efficient implementation of the new algorithm is presented, and its performance is discussed on the basis of tests conducted with data from the Danish high resolution C-band SAR [1]. Finally, a few conclusions are made.

MAP DRIFT

The map drift algorithm [2] is based on the fact that two or more looks misregister in the azimuth direction if they are processed with an incorrect Doppler rate. When two looks are formed by dividing the Doppler spectrum into two spectral bands separated in time by τ, the temporal misregistration δ_{md} is

$$\delta_{md} = -\frac{\tau\Delta\dot{f}}{\dot{f}_f} = C\Delta\dot{f} \tag{2}$$

$\Delta\dot{f}$ is the difference between the correct Doppler rate $\dot{f}$ and the Doppler rate $\dot{f}_f$ of the matched filter

$$\Delta\dot{f} = \dot{f} - \dot{f}_f = \frac{-2}{\lambda R}\left((v_f + \Delta_v)^2 - v_f^2\right) \tag{3}$$

Likewise $\Delta_v = v - v_f$ is the difference between the correct along track velocity v and that assumed in the processing v_f.

In order to estimate the misregistration the two looks are focused, detected and cross-correlated in azimuth on a line by line basis. Several cross-correlation functions from adjacent ranges are accumulated, and the result has a peak at δ_{md}. The size of the peak depends on the scene contrast.

Knowing δ_{md}, $\Delta\dot{f}$ can in principle be found from Eq. 2 and subsequently Δ_v from Eq. 3. However, the coefficient C is not easily computed because the effective Doppler bandwidth B_D, and hence the temporal look separation, are not known exactly.

Instead, the entire procedure is repeated a number of times. The peak position is measured for a few different filter velocities,

and a linear regression provides the estimate of the velocity for which $\delta_{md} = 0$. This approach also reduces the uncertainty of the peak position determination as well as the effect of the stochastic nature of the scene.

Fig. 1 illustrates the algorithm. It is assumed that the autofocus is part of a range-Doppler SAR processing with the matched filtering implemented in the frequency domain. In this case the Doppler spectrum is computed anyway, and therefore the corresponding Fast Fourier Transform (FFT) is disregarded.
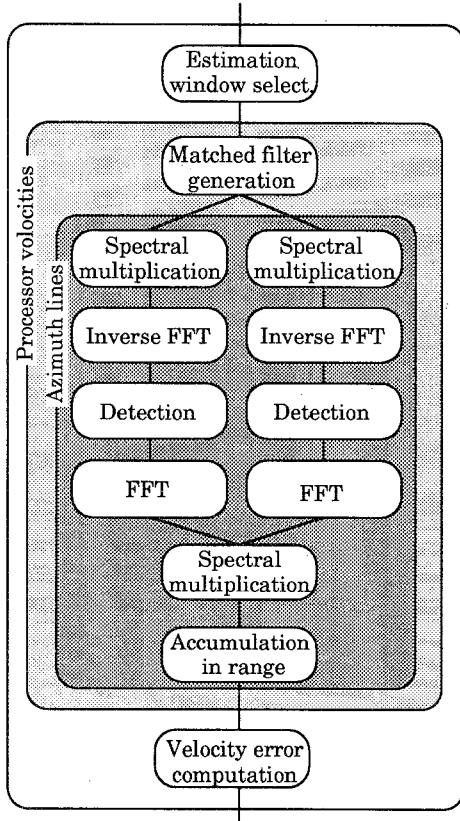

Fig. 1. Map drift block diagram.

Table 1 evaluates the computational complexity for an $N_r \times N_a$ estimation window (range samples × azimuth samples). $N_a = 2048$, and the figures are normalized by N_r. Only two different processing velocities are assumed.

Operation	real adds.	real mults.
matched filter generation	≈ 0	≈ 0
spectral multiplication	8192	16384
FFT^{-1}	270336	180224
detection	8192	16384
correlation (FFT, mult.)	139264	98304
accumulation in range	2048	0
D$_v$ computation	≈ 0	≈ 0
In total	428032	311296

Table 1. Computational complexity of map drift.

SHIFT - AND - CORRELATE (SAC)

Like the above-mentioned map drift, the new shift-and-correlate algorithm forms two signals (looks), s_l and s_u, the spectra of which are respectively the lower half and the upper half of the original Doppler spectrum. The name of the algorithm refers to the fact that the signals are frequency shifted relative to one another and subsequently cross-correlated. Contrary to the map drift the two looks are not focused and detected before the correlation.

The cross-correlation leads to a pulse compression as illustrated in Fig. 2. Only the relative frequency shift is of importance, and the following derivation becomes clearer if s_l and s_u are shifted by $+f_{PRF}/4$ and $-f_{PRF}/4$, respectively. f_{PRF} is the Pulse Repetition Frequency after the azimuth pre-summing (if applied). The Doppler signal from a point target at $x_a = vt_a$ is considered

$$s = \exp(\phi_a)\, \exp(\pi \dot{f}(t - t_a)^2)\,, \qquad t_a - \frac{T}{2} < t < t_a + \frac{T}{2} \qquad (4)$$

Here $T = B_D / |\dot{f}|$. The amplitude factor of the Doppler signal has been neglected for simplicity. It has no impact on the position of the correlation maximum.
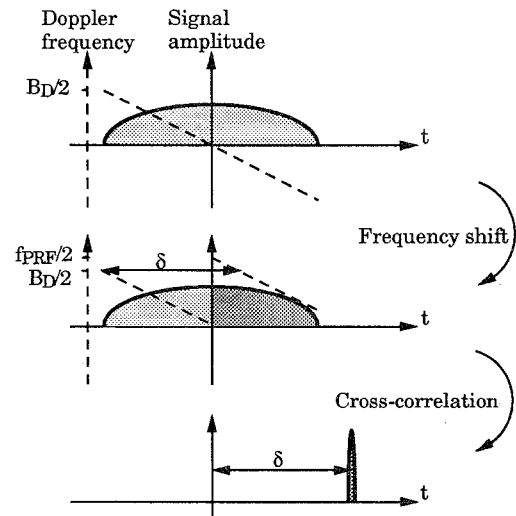

Fig. 2. Shift -and-correlate principle.

The two frequency shifted looks are given by

$$s_{l+} = s_l\, \exp\!\left(\frac{\pi}{2} f_{PRF} t\right) \approx \exp\!\left(\phi_a - \pi \dot{f} \delta t_a - \pi \dot{f}\!\left(\frac{\delta}{2}\right)^{\!2}\right) \exp\!\left(\pi \dot{f}\!\left(t - t_a - \frac{\delta}{2}\right)^{\!2}\right)$$

$$t_a < t < t_a + \frac{T}{2} \qquad (5)$$

$$s_{u-} = s_u\, \exp\!\left(-\frac{\pi}{2} f_{PRF} t\right) \approx \exp\!\left(\phi_a + \pi \dot{f} \delta t_a - \pi \dot{f}\!\left(\frac{\delta}{2}\right)^{\!2}\right) \exp\!\left(\pi \dot{f}\!\left(t - t_a + \frac{\delta}{2}\right)^{\!2}\right)$$

$$t_a - \frac{T}{2} < t < t_a \qquad (6)$$

$$\delta = \frac{f_{PRF}}{2|\dot{f}|} \qquad (7)$$

Here the stationary phase approximation to an ideally band-pass filtered linear FM signal is applied. The cross-correlation is

$$s_c = \exp(2\pi \dot{f} \delta t_a)\, s_p(t - \delta) \qquad (8)$$

where s_p is the usual sinc-like pulse compressed linear FM signal with bandwidth $B_D/2$. No image is formed by the correlation

1070

because the maximum appears at $t = \delta$ irrespective of the point target position t_a. This means that the cross-correlations for all targets at the same range coincide. The Doppler rate, and thereby the velocity, is given by the position of the correlation maximum through Eq. 7. Unlike the absolute target phase ϕ_a, the position dependent phase in Eq. 8 does not cancel, and therefore the correlation contributions do not add up coherently.

So far, only the desirable contributions to the cross-correlation function have been considered. However, s_l from the target at t_a also correlates with s_u from another target at t_b and gives a contribution at $t = \delta + t_b - t_a$. In general all target pairs separated in time by $t_b - t_a$ gives a peak at this point.

Still, a correlation maximum appears at δ if the scene is inhomogeneous. The mechanism is similar to that ensuring a correlation peak in the map drift algorithm. The square law detected cross-correlation generated in the shift-and-correlate algorithm can be considered a non-stationary stochastic signal (gamma distribution), the ensemble average of which is a function of time. For a given scene contrast this ensemble average can be shown to be directly proportional to the amplitude of the correlation function that is computed in the map drift algorithm. In particular, the ratio of the ensemble average at $t = \delta$ to the ensemble average at $t \neq \delta$ ("signal-to-clutter ratio") is the same in the two algorithms.

However, the gamma distribution has a high variance, and so the shift-and-correlate algorithm must accumulate a number of detected cross-correlation functions from adjacent ranges in order to avoid that the peak fades out. The phenomenon is similar to the speckle noise in SAR images.

The accumulation of cross-correlation functions also reduces the effect of the stochastic nature of the scene. However, this can advantageously be accomplished by an accumulation of complex cross-correlation functions. There is a great computational advantage in keeping the number detections low.

The range accumulation has to take into account that the position of the correlation peak is proportional to the range, cf. Eq. 7. Otherwise a smearing occurs. The peak position should be determined with an accuracy of

$$\frac{\partial(T/2)}{\partial v}\rho_v = \pm \frac{\partial}{\partial v}\left(\frac{f_{PRF}\lambda R}{4v^2}\right)\frac{v\rho_a^2}{\lambda R} \approx \frac{\pm 1}{2f_{PRF}}\frac{\rho_a^2}{\Delta_a^2} \quad (9)$$

in order to estimate the velocity with the accuracy required by Eq. 1. $\Delta_a = v/f_{PRF}$ is the azimuth sample spacing, which equals ρ_a for $B_D = f_{PRF}$. So, according to Eq. 9 the peak position should be known within approximately one sample. (The same accuracy is required for δ_{md} in the map drift algorithm.) The range interval Δ_{Rs} over which the peak position changes one sample is found from Eq. 7

$$\Delta_{Rs} = \frac{2\Delta_a^2}{\lambda} \quad (10)$$

Not surprisingly, Δ_{Rs} is equal to the depth of focus. They both specify the range interval, within which the Doppler rate can be considered constant.

It is desirable to accumulate over a larger range interval, and therefore the cross-correlation functions are time shifted by

$$\delta_s = -\frac{f_{PRF}}{|f_f|} \quad (11)$$

to an approximately zero offset. It is noted that this is the only point in the algorithm, where an a priori estimate of the platform velocity v_f is needed.

The maximum range interval over which the accumulation of the time shifted cross-correlation functions can extend without smearing is

$$\Delta_{Ra} = \left(\frac{\lambda}{2}f_{PRF}^2\left(\frac{1}{\left(v_f+\Delta_v\right)^2} - \frac{1}{v_f^2}\right)\right)^{-1} \approx \frac{\Delta_a^2}{\lambda}\frac{v_f}{\Delta_v} \quad (12)$$

provided that the velocity is known within Δ_v.

SAC IMPLEMENTATION

Fig. 3 illustrates the shift-and-correlate algorithm, and Table 2 evaluates the computational complexity for an $N_r \times N_a$ estimation window. Again the number of arithmetic operations is normalized by N_r. N_a is 2048, the detection rate is once per 32 cross-correlations, and the time windows are 128 samples.
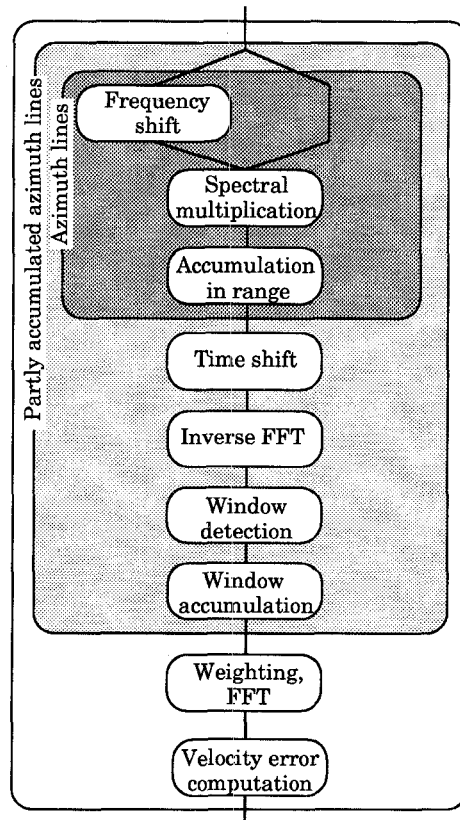

Fig. 3. Shift-and-correlate block diagram.

Operation	real adds.	real mults.
frequency shift	0	0
cross-correlation	2048	4096
complex accumulation	2048	0
time shift	64	128
detection (incl FFT^{-1})	2116	1416
window accumulation	≈ 0	≈ 0
weighting, FFT, D_v comp	≈ 0	≈ 0
In total	5576	6340

Table 2. Computational complexity of SAC.

1071

The frequency shift is merely an array indexing, and the cross-correlation translates into a multiplication of the upper half of the spectrum by the complex conjugate of the lower half.

It has been found that the standard deviation of the velocity estimates increases when less than about 8 detected accumulations are added, whereas no significant advantage is obtained by a more frequent detection. Still, it is convenient to confine the complex accumulation to a range interval equal to the depth of focus Δ_{Rs}, even in cases where Δ_{Rs} is less than $N_r/8$ range samples. This leads to a simpler computational structure, because the detections are then accompanied by the time shifts as shown in Fig. 3.

The time shifts are implemented as a spectral multiplication by a phase ramp, the slope of which is proportional to δ_s.

The detection involves an inverse Fast Fourier Transform (FFT) and a square law detection of a "window" of the complex time signal. The signal bandwidth is halved by the initial cross-correlation, but doubled by the detection. Consequently, the inverse Fourier transform must be applied to the full bandwidth (zero padding) in order to avoid aliasing.

The accumulation of the detected windows takes place in the time domain. Therefore a single FFT suffices to return to the frequency domain, where the position of the correlation peak is determined from the phase slope α. The weighted time windowing reduces the spectral noise.

Finally the velocity error Δ_V is computed from

$$-\frac{\alpha}{2\pi} = \delta - \delta_s = \frac{\lambda R f_{PRF}}{4}\left(\frac{1}{(v_f + \Delta_v)^2} - \frac{1}{v_f^2}\right) \qquad (13)$$

DISCUSSION

The shift-and-correlate algorithm has been applied to two different scenes acquired with the Danish SAR: A) a city centre, and B) a suburbia including lakes, and a deer garden. Tests with agricultural areas and forests have not yet been conducted. Fig. 4 shows a correlation peak (after range accumulation) typical of scene B, and Fig. 5 shows the corresponding spectral phase.

In both cases estimates have been obtained from adjacent sub-scenes covering the entire scene. Table 3 compares the standard deviation of the velocity estimates with the accuracy needed in order to achieve a maximum quadratic phase error of $\pi/4$.
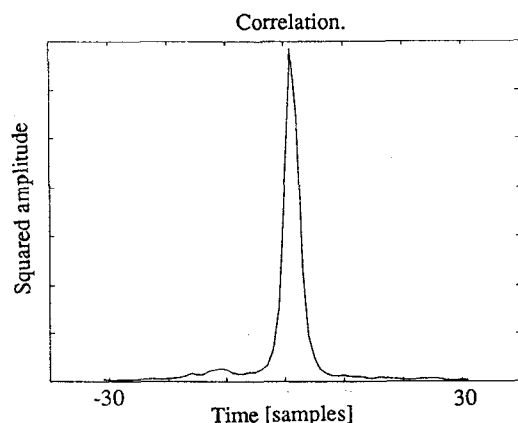
Correlation.

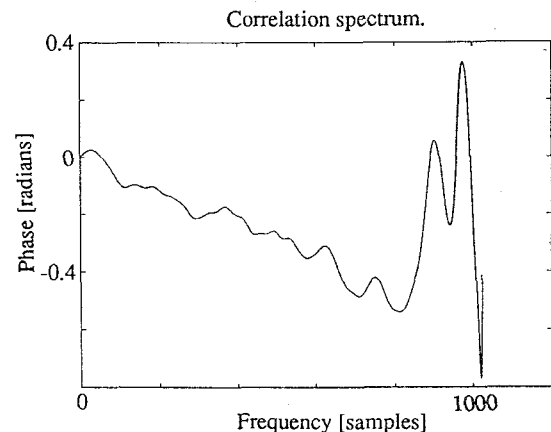Fig. 4. Correlation peak.

Correlation spectrum.

Fig. 5. Spectral phase.

Preliminary tests indicate that the map drift provides velocity estimates with 10 to 25 per cent smaller standard deviation.

A weighting by the correlation peak amplitudes is recommendable, as small amplitudes tends to correspond to estimates deviating significantly from the average.

	Scene A	Scene B
Standard dev.	0.38 m/s	0.55 m/s
ρ_V cf. Eq. (1)	± 0.60 m/s	± 0.89 m/s

Table 3. SAC performance.

CONCLUSIONS

A new autofocus algorithm with a very low computational complexity has been presented. Although based on a completely different principle, this "shift-and-correlate" algorithm has some similarity with the traditional map drift algorithm. Theoretically the two algorithms have comparable accuracies. Preliminary tests with a high contrast scene indicate that the map drift velocity estimates have a 10 to 25 per cent smaller standard deviation, but both algorithms meet the requirement to a maximum quadratic phase error of $\pi/4$. The shift-and-correlate algorithm is less sensitive to the a priori velocity estimate, and, most importantly, it calls for about 50 times fewer arithmetic operations. It is a single-pass algorithm unlike the map drift and the class of contrast optimization algorithms, which are all iterative. Therefore the algorithm is very suitable for real-time processing, and it can be applied to the entire imagery, not only to sub-windows. The Danish high resolution real-time processor [3], which is expected to be operational early 1992, is likely to adopt the shift-and-correlate algorithm.

REFERENCES

[1] S.N. Madsen, E.L. Christensen, N. Skou, J. Dall, "The Danish SAR System; Design and Initial Tests", accepted for publication in IEEE Transactions on Geoscience and Remote Sensing.

[2] J.C. Curlander, C. Wu, A. Pang, "Automated preprocessing of spaceborne SAR data", Proceedings of IGARSS'82, pp. FA-1/3.11-6, Munich, June 1982.

[3] J. Dall, J.H. Jørgensen, E.L. Christensen, and S.N. Madsen, "A real-time processor for the Danish C-band SAR", Proceedings of IGARSS'91, Helsinki, June, 1991.